Detection of Xylene as a Detrimental Chemical Compound by Employing a Photonic Crystal Based on Porous Silicon

Sofyan A. Taya‡, Nael Doghmosh, Anas A. M. Alkanoo

Physics Department, Islamic University of Gaza, P.O. Box 108, Gaza, Palestine.

(staya@iugaza.edu.ps, ndoghmosh96@gmail.com, akanoo@iugaza.edu.ps)

‡ Corresponding Author; Sofyan A. Taya, staya@iugaza.edu.ps

Received: 28.02.2023 Accepted:29.03.2023

Abstract- An optical sensor based on a one-dimensional binary photonic crystal (PC) with an inverted symmetry has been proposed for the detection of Xylene which is a harmful chemical compound. The structure of the PC is considered $(Si/ SiO_2)^N (SiO_2/ Si)^N$, where N is the number of unit cells and Si is considered porous. The analyte material is assumed to be infiltrated into the silicon porous network. The transfer matrix method is used to analyze the PC structure. The refractive index of the porous Si layer as a function of the layer liquid fraction and porosity has been investigated. The sensor performance parameters such as the sensitivity, quality factor, detection limit and detection accuracy have been studied. The variation of these parameters has been examined with varying Si porosity, layer liquid fraction, porous layer thickness, and angle of incidence. It has been found that a sensitivity of 812.042 can be obtained at an incidence angle of 70°, a silicon porosity of 0.75, and a thickness of the porous silicon layer of 650 nm. The proposed sensor can become a milestone for the detection of gases and liquids for industrial purposes.
Keywords: Photonic crystal; porous silicon, chemical sensor; Xylene.

1. Introduction

Porous silicon's intriguing optical characteristics have been of interest to physicists, chemists and engineers. Due to the large refractive index (RIX) fluctuation caused by controlling the porosity, the relatively simple fabrication processes, and the low manufacturing costs, porous silicon is an extremely intriguing prospect for photonic applications. Porous silicon is often produced by the electrochemical dissolving of silicon wafers in ethanol/HF or aqueous solution [1]. Many researchers have explored the development of 1D photonic crystal (PC) based on porous silicon for both the near-infrared and visible spectra. The characteristics of these PCs have been investigated as well. Porous PCs have attracted a lot of interest in the field of chemical sensing because they offer the chance to observe compound separation and recognition through the optical response change generated by the presence of targeted species [2-4]. Many of these achievements have been accessible because of the presence of a porous network in ordered 3D packings of monodisperse [5-7]. Few 2D PCs have accessible ordered porosity on the outside. This characteristic permits the optical response to be controlled by the ambient conditions [3]. Recently, new types of 1D PCs with controlled porosity have been proposed by alternatively depositing thin layers that are mesostructured [8] or nanoparticle-based [9]. The structure of 1D PC exhibits very wide and powerful Bragg reflections and is often simpler to construct than those of higher dimensions. The many different materials that can be deposited as layers, implying precise control over the periodic ensemble's optical properties, the high structural and optical quality that can be attained, and the ease with which they can be functionalized and integrated into devices are all advantages of these lattices [4]. Through the infiltration of several liquid types, the environmental response of these lattices has been studied [8].

One of the most fruitful areas of research in optoelectronics and optics is the control of light propagation [10]. For the design of optical and optoelectronic devices, nanoscale research is receiving a lot of attention these days [11]. A multilayer of dielectric materials with low and high RIXs makes up a photonic crystal (PC), which regulates the propagation of light [12]. PCs can be divided into binary, ternary, quaternary, and other types according to how many layers are present in a single period. To build a PC, one period has to be repeated N times. The presence of a photonic band gap (PBG) in the transmission spectra of a PC is the main feature of such structures [13]. PCs have therefore been extensively used in a variety of applications, including optical mirrors [14], filters [15], absorbers [16] and optical sensors [17]. One of the most significant applications of a PC is as a

sensor. It can be employed efficiently as a chemical sensor [18], temperature sensor [19], biosensor [20], pressure sensor [21] and gas sensor [22].

Xylene is an organic compound. It has three isomers: 1,2-dimethylbenzene (ortho-xylene abbreviated as o-xylene), 1,3-dimethylbenzene (meta-xylene abbreviated as m-xylene), and 1,4-dimethylbenzene (para-xylene abbreviated as p-xylene). It has the chemical formula $(CH_3)_2C_6H_4$. Xylene is produced when two hydrogen atoms in a benzene ring are replaced with methyl groups; depending on which hydrogens are replaced, one of three structural isomers is produced [23]. Catalytic reforming and coal carbonization both yield xylene which is an essential petrochemical. It can also be found in crude oil in amounts of 0.5% to 1%. Tiny amounts can be found in gasoline and aircraft fuels. Each year, many million tons are produced. Dimethyl terephthalate and terephthalic acid, two monomers used to make polyethylene terephthalate plastic bottles and polyester clothing, are mostly derived from p-xylene [24]. Leather, rubber, and the printing industries all employ xylenes as solvents. It is a typical ingredient in rubber, adhesives, and ink. It can be used instead of toluene to thin paints when a slower drying time is preferred. As a cleaning agent, it can be used on silicon wafers and integrated circuits. In the lab, xylene is used as a solvent to remove synthetic immersion oil from the microscope objective in light microscopy and to create dry ice baths to chill reaction vessels. Xylene is toxic and oxidation to produce methylbenzoic acid and hydroxylation to produce hydroxylene are the two main detoxifying mechanisms. The primary consequence of inhaling xylene vapor is central nervous system depression with symptoms such as vomiting, nausea, lightheadedness and headache [23,24]. A headache or nausea may occur at an exposure level of 100 ppm. Symptoms can include vomiting, weakness, dizziness, irritability and delayed reaction time at exposure levels between 200 to 500 ppm [23,24].

The study presented here focuses on using a binary PC with a porous silicon foundation as a chemical sensor for the Xylene compound as a harmful chemical material. The PC used in this article has the structural formula $(\alpha\beta)^N(\beta\alpha)^N$, where α layer is Si and β layer is SiO_2 are the two materials of the PC. The silicon used here is porous and the Xylene analyte is infiltrated into the porous network of silicon. The transfer matrix (TrM) method is used to analyze the binary PC. The effective RIX of the silicon increases as a result of the flow of Xylene in the porous network. The main idea of the sensor is the detection of the defect mode shift due to this change in the effective RIX.

2. Transfer matrix technique

In Fig. 1, the proposed binary PC is displayed. It comprises two media that are arranged one on top of the other and has an inverted symmetry. The two media are repeated N times as $(\alpha\beta)^N$ in the first half and as $(\beta\alpha)^N$ in the second half. The final PC structure is $(\alpha\beta)^N(\beta\alpha)^N$. The two layers are occupied by Si and SiO_2 with RIXs n_1 and n_2 and thicknesses d_1 and d_2. The TrM technique is effective for manipulating such structures. The TrM of a single layer has the following formula

$$M = \begin{bmatrix} cos\theta_i & -(j/\sigma_i)sin\theta_i \\ -\sigma_i sin\theta_i & cos\theta_i \end{bmatrix} \quad (1)$$

where i denotes the layer order,
$\theta_i = (2\pi/\lambda)n_i d_i cos\omega_i$ is the phase shift,
n_i is the RIX of the layer,
d_i is the thickness,
θ_i is the layer angle of incidence.

The angle θ_i can be written as

$$cos\theta_i = \sqrt{1 - (sin^2\theta_0)/n_i^2} \quad (2)$$

where θ_0 is the ambient incidence angle.

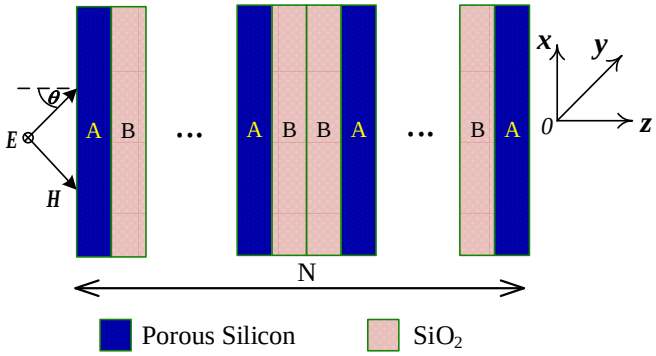

Figure 1. A PC consisting of two layers in an inversion symmetry.

The TrMs for layers α and β are designated as M_α and M_β. The TrMs for the combinations $\alpha\beta$ and $\beta\alpha$ are given by $M_{\alpha\beta} = M_\alpha M_\beta$ and $M_{\beta\alpha} = M_\beta M_\alpha$, respectively. The pair of layers in the first half is $\alpha\beta$ and in the second half is $\beta\alpha$. The total TrM of an inverted symmetry PC can be written as

$$M_T = (M_{\alpha\beta})^N (M_{\beta\alpha})^N = \begin{bmatrix} M_{11} & M_{12} \\ M_{21} & M_{22} \end{bmatrix} \quad (3)$$

The M_T matrix elements can be used to express the reflection coefficient as

$$r = \frac{(M_{11}+M_{12}\eta_{out})\phi_{in} - (M_{21}+M_{22}\eta_{out})}{(M_{11}+M_{12}\eta_{out})\phi_{in} + (M_{21}+M_{22}\eta_{out})} \quad (4)$$

where $\eta_{out} = \eta_{in} = cos\theta_0$ since the PC is assumed to be surrounded by air. The reflectance can be expressed as follows using the reflection coefficient

$$R = |r|^2 \quad (5)$$

Porous silicon is regarded as an efficient medium with a dielectric function (ε_{pry}) that is midway between that of silicon (ε_{si}) and that of air (ε_{air}) in the visible frequency range. Making Use of the Bruggeman approximation [25],

$$(1-Pr)\left(\frac{\varepsilon_{si}-\varepsilon_{pry}}{\varepsilon_{si}+2\varepsilon_{pry}}\right) + (Pr-\delta)\left(\frac{\varepsilon_{air}-\varepsilon_{pry}}{\varepsilon_{air}+2\varepsilon_{pry}}\right) + \delta\left(\frac{\varepsilon_{ch}-\varepsilon_{pry}}{\varepsilon_{ch}+2\varepsilon_{pry}}\right) = 0 \quad (6)$$

where Pr is layer porosity,
δ is layer liquid fraction,

ε_{pry}, ε_{ch}, ε_{air}, and ε_{si} are dielectric constants of porous silicon, chemical to be infiltrated into the pores, air, and silicon, respectively.

A sensor performance can be evaluated by using a set of parameters. Sensitivity (S), quality factor (QF), detection limit (DL) and detection accuracy (DA) are the well-known metrics. How the sensor is efficient can be calculated using these factors. These characteristics can be calculated using these mathematical formulas [26]

$$S = \frac{\Delta\lambda_R}{\Delta n_e} \quad (7)$$

$$QF = \frac{\lambda_R}{FWHM} \quad (8)$$

$$DL = \left(\frac{2\Delta n_e}{3}\right)\left(\frac{FWHM}{\Delta\lambda_R}\right)^{1.25} \quad (9)$$

$$DA = \frac{1}{\text{FWHM}} \quad (10)$$

where $\Delta\lambda_R$ and Δn_e are the resonant peak wavelength and RIX changes.

3. Numerical results

In this study, the potential of a 1D PC with inverted symmetry as a chemical sensor is explored. The structure that is used here has the composition $(Si/ SiO_2)^N$ $(SiO_2/ Si)^N$, where Si is considered porous. N = 10 is the number of unit cells. When Xylene is injected into the porous structure, the chemical compound with a higher RIX replaces the air inside the void area of the ensemble, changing the effective RIX of the whole material. As a result, it is anticipated that the Bragg peak would redshift. The transmission spectrum tuning can precisely identify the sort of chemical component that is present in the silicon pores and determine its RIX. The sensitivity of the suggested device is significantly influenced by the Si porosity and the layer liquid fraction (δ). When δ is equal to a number greater than zero, the chemical compound partially fills the Si pores, which are otherwise completely filled with air when δ = 0. The structural parameters are set to d_1 = 300 nm, d_2 = 130 nm, P = 0.62 [25], θ_o = 0, and δ = various values. The RIX of Xylene is 1.501 [27]. The layer liquid fraction and porosity, which have a significant impact on the RIX of porous silicon ($n_{pry} = \sqrt{\varepsilon_{pry}}$), are the key factors. Figure 2 depicts a 3D plot of the porous silicon RIX vs porosity and layer liquid fraction. The graph demonstrates that when the porosity is at its maximum value and δ = 0, the RIX is at its lowest value. The RIX begins to rise as δ rises above zero and reaches its peak when the porosity is minimum and δ has the highest value.

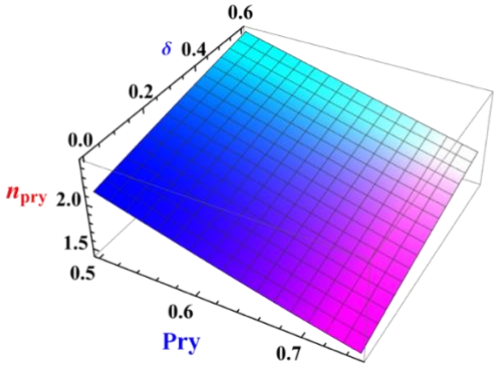

Figure 2. A 3D plot of the refractive index of the porous Si layer as a function of layer liquid fraction (δ) and the porosity (Pry).

The performance of the chemical sensor is examined in the next subsections when varying the layer liquid fraction, incidence angle, thickness, and porosity of the porous silicon. To improve the performance of the chemical sensor, certain parameters must be tuned.

3.1. Layer liquid fraction

When the chemical component partially fills the pores, the layer liquid fraction value becomes greater than zero. As demonstrated by Eq. (6), when the layer liquid fraction changes, the RI of porous silicon also changes, which affects the effective RIX of the structure. Figure 3 shows the transmission spectra when infrared radiation of wavelength 700 – 850 nm is incident and the layer liquid fraction changes from 0 to 0.6. The resonant peak moves toward a longer wavelength as the layer liquid fraction rises. The redshift is due to the RIX rise of the porous silicon as δ increases. Table 1 shows the performance parameters for the porous Si sensor when δ changes. The variation of these performances as a function of layer liquid fraction is depicted in Figure 4. As the layer liquid fraction increases, the FWHM dramatically decreases and the resonant peak sharpens. This can raise the quality factor of the sensor. The quality factor is 27200 when the layer liquid fraction approaches 0.6. For sensing applications, the high-quality factor is preferred. When the layer liquid fraction rises, the sensitivity, a crucial performance measure, slightly decreases. The detection limit, which decreases as the layer liquid fraction rises, is the lowest index change that may be detected. The reciprocal of the FWHM yields detection accuracy (DA). The sensor performs better when the FWHM is minimum and the DA is maximum. As δ rises from 0 to 0.6, the DA changes from 1.2 to 32.89, which means a considerable improvement. Examination of Table 1 and Fig. 4 reveals that FWHM and DL both decrease as the layer liquid fraction rises. On the other hand, as the layer liquid fraction rises, QF and DA increase. In general, the sensor's performance is enhanced as the layer liquid percentage increases.

Figure 3. Transmission spectra for various δ values when Xylene is the analyte.

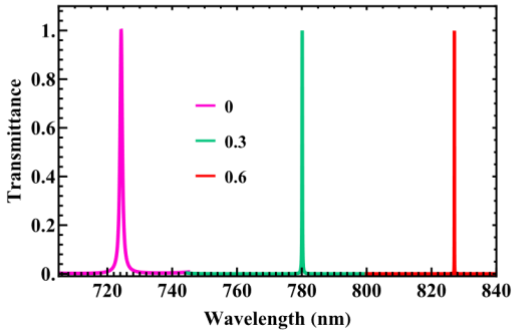

Table 1. Defect mode position, full width, sensitivity, quality factor, detection limit and detection accuracy of the proposed sensor for various values of δ.

δ	λ_c (nm)	FWHM (nm)	S × 10^2 (nm/RIU)	QF × 10^3	DL×10^{-3}	DA (nm^{-1})
0	724.3	0.832	-	0.9	-	1.2
0.1	744.1	0.426	2.87	1.7	0.38	2.35
0.2	762.6	0.228	2.84	3.3	0.15	4.39
0.3	780.1	0.128	2.812	6.1	0.07	7.83
0.4	796.6	0.075	2.786	10.6	0.03	13.28
0.5	812.2	0.047	2.762	17.4	0.02	21.41
0.6	827.	0.03	2.74	27.2	0.01	32.89

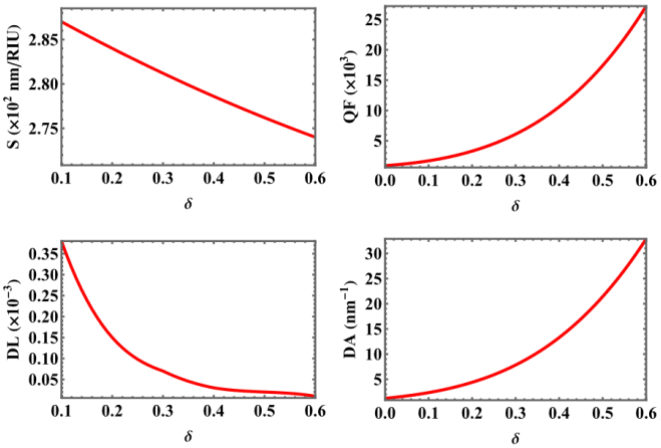

Figure 4. Performance parameters as a function of δ for the Xylene analyte.

3.2. Incidence angle

Optimizing the structure parameters to maximize the sensitivity is the main aim because it's the most important performance parameter. In the following, δ is taken 0.1 since it corresponds to the highest sensitivity. The incident angle that corresponds to the highest sensitivity will be found. In Table 2, the performance parameters and the resonant wavelength are reported with the variation of the incident angle. The variation of the performance parameters versus the angle of incidence is depicted in Figure 5. With an increase in the incident angle, the FWHM shows a significant drop, which means that the resonant peak becomes sharper. This has the potential to significantly raise the quality factor. The quality factor is 1700 when the incidence angle is 0°. The quality factor changes to 32800 at a 70° incident angle. As the incidence angle rises from 0° to 70°, the sensitivity increases from 287 to 314.7 nm/RIU. The detection limit decreases form 0.38×10^{-3} at θ_0 = 0° to 0.01×10^{-3} at θ_0 = 70°. The chemical sensor performs better when the detection limit value is lower. As the FWHM goes lower, the DA gets higher and the chemical sensor works better. The DA improves from 2.35 to 53.14 as the incidence angle rises from 0° to 70°. Looking at Table 2 and Fig. 5 reveals that FWHM and DL values drop as the angle of incidence increases, which is encouraging. On the other side, as the incidence angle increases, the sensitivity, QF and DA are all improved. With the increase of the incidence angle, the sensor performance is significantly improved.

Table 2. Defect mode position, full width, sensitivity, quality factor, detection limit and detection accuracy of the proposed sensor for various angles of incidence.

θ_o (°)	λ_c (nm)	FWHM (nm)	S × 10^2 (nm/RIU)	QF × 10^3	DL×10^{-3}	DA (nm^{-1})
0	744.1	0.426	287.0	1.7	0.38	2.35
10	740.2	0.4	287.9	1.8	0.35	2.5
20	728.8	0.331	290.6	2.2	0.27	3.02

30	711.	0.24	294.7	3.	0.18	4.17
40	688.4	0.152	299.8	4.5	0.1	6.58
50	663.4	0.084	305.3	7.9	0.05	11.84
60	638.7	0.043	310.6	14.8	0.02	23.11
70	617.5	0.019	314.7	32.8	0.01	53.14

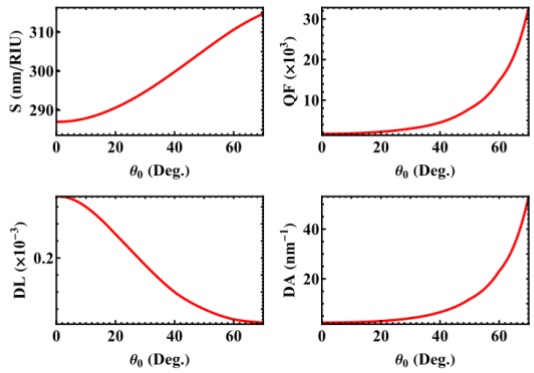

Figure 5. Performance parameters as a function of θ_0 for the Xylene analyte.

3.3. Thickness of the porous silicon

The impact of porous silicon layer thickness (d_1) on the sensor performance will be studied. Both the layer liquid fraction and the incidence angle remain unchanged at 70° and 0.1, respectively. Table 3 shows the relationship between the variation of the porous silicon layer thickness and the variation of the resonant wavelength and all performance parameters. Figure 6 shows how the performance characteristics vary depending on the thickness of the porous silicon layer. With an increase in d_1, the FWHM increases, indicating that the resonant peak widens. The quality factor is 183500 at d_1 = 300 nm, and it is 4400 at d_1 = 650 nm. The sensitivity significantly improves when d_1 grows from 300 to 650 nm, going from 318 to 698.6 nm/RIU. At d_1 = 300 nm, the detection limit is 0.075645×10^{-5}, and it rises to 6.54282×10^{-5} when d_1 = 650 nm. The DA decreases from 306.14 to 3.93 when d_1 grows from 300 nm to 650 nm. The huge improvement in the sensor sensitivity is, in our opinion, the most important consequence of increasing the thickness of the porous silicon layer.

Table 3. Defect mode position, full width, sensitivity, quality factor, detection limit and detection accuracy of the proposed sensor for various values of d_1.

d_1 (nm)	$\lambda_c \times 10^3$ (nm)	FWHM (nm)	$S \times 10^2$ (nm/RIU)	$QF \times 10^3$	$DL\times10^{-5}$	DA (nm^{-1})
300	0.6	0.003	3.18	183.5	0.075645	306.14
320	0.63	0.004	3.348	149.5	0.097070	238.18
340	0.66	0.006	3.526	118.7	0.128277	180.97
360	0.68	0.008	3.717	90.6	0.177397	132.45
380	0.71	0.01	3.915	68.4	0.248894	95.9
400	0.74	0.014	4.121	51.5	0.349534	69.44
420	0.77	0.02	4.333	39.0	0.487027	50.65
440	0.8	0.027	4.551	29.9	0.669506	37.39
460	0.83	0.036	4.772	23.2	0.904989	28.01
480	0.86	0.047	5.005	18.3	1.19852	21.33
500	0.89	0.061	5.224	14.7	1.56338	16.52
550	0.96	0.107	5.805	9.0	2.78343	9.37
600	1.04	0.171	6.393	6.1	4.45955	5.84
650	1.12	0.254	6.986	4.4	6.54282	3.93

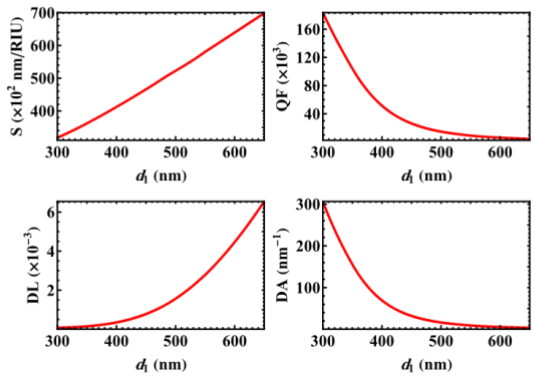

Figure 6. Performance parameters as a function of d_1 for the Xylene analyte.

3.4. Silicon layer porosity

One important factor that could significantly impact the performance of the device is the porosity. The impact of porosity on the performance parameters of the suggested chemical sensor is examined in this section. Table 4 reports the variation of FWHM, sensitivity, QF, DL and DA with the silicon layer porosity. The performance parameters variation versus the silicon layer porosity is depicted in Figure 7. The sensitivity significantly improves when the porosity rises from 0.5 to 0.75, going from 678.201 nm/RIU to 812.042 nm/RIU. The QF displays a decline as the porosity increases due to the widening of the FWHM. The DL shows a minimum and the DA shows a maximum at P = 0.56.

Table 4. Defect mode position, full width, sensitivity, quality factor, detection limit and detection accuracy of the proposed sensor for various values of the Si porosity.

P	$\lambda_c \times 10^3$ (nm)	FWHM (nm)	$S \times 10^2$ (nm/RIU)	QF $\times 10^3$	DL$\times 10^{-3}$	DA (nm^{-1})
0.5	1.35	0.269287	6.78201	5.02475	0.074899	3.71
0.56	1.23	0.240329	6.8492	5.13546	0.063168	4.16
0.62	1.12	0.254344	6.98562	4.38423	0.065428	3.93
0.65	1.06	0.296611	7.10765	3.56056	0.077368	3.37
0.68	1.	0.392169	7.29155	2.5438	0.106162	2.55
0.71	0.94	0.603704	7.5653	1.55656	0.174111	1.66
0.72	0.92	0.722269	7.68207	1.27446	0.21395	1.38
0.73	0.9	0.878753	7.81343	1.02577	0.268003	1.14
0.75	0.86	1.35825	8.12042	0.63553	0.441669	0.74

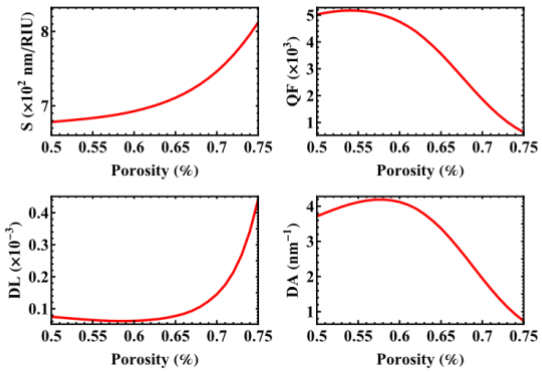

Figure 7. Performance parameters as a function of the Si porosity for the Xylene analyte.

In Table 5, the sensitivity of the current research is compared with recent work on chemical and biochemical sensors. The current sensor has attained the utmost sensitivity.

Table 5. Comparison between the current work sensitivity and recently published chemical and biochemical sensors.

Ref.	**S** (nm/RIU)	**Publishing Year**
[28]	436	2011
[29]	18.8	2015
[30]	727.27	2017
[31]	476	2020
[32]	11.9	2020
[33]	144.369	2022
Current work	812. 042	2022

4. Conclusion

Xylene is toxic and the primary consequence of inhaling xylene vapor is central nervous system depression with symptoms such as vomiting, nausea, lightheadedness and headache. In this work, a Xylene sensor based on a one-dimensional PC with inverted symmetry has been introduced. The PC structure $(Si/ SiO_2)^N$ $(SiO_2/ Si)^N$ was employed, where silicon is porous. The effective RIX of the structure is improved when the analyte is incorporated into the porous network of the silicon material. As a result, the Bragg peak is seen to redshift. The performance parameters of the proposed sensor have been thoroughly examined. Many interesting findings have been observed. Most of the performance parameters rise as the layer liquid fraction increases. With an increase in the incident angle, all the performance parameters significantly improve. The most important performance parameter is sensitivity. Increasing the incidence angle, silicon porosity, and thickness of the porous silicon layer, can greatly improve the sensitivity. An incidence angle of 70°, a silicon porosity of 0.75, and a thickness of porous silicon layer of 650 nm correspond to the maximum sensitivity. A sensitivity of 812.042 has been obtained. The proposed PC can become a milestone for the detection of liquids and gases for industrial purposes.

References

[1] J. Clerk Maxwell, A Treatise on Electricity and Magnetism, 3rd ed., vol. 2. Oxford:Clarendon Press, 1892, pp.68-73. (Book)

[2] N. Hidalgo, M. E. Calvo, S. Colodrero, and H. Míguez, “Porous One-Dimensional Photonic Crystal Coatings for Gas Detection”, *IEEE Sens. J.*, Vol. 10, No. 7, pp. 1206-1212, 2010.

[3] C. F. Blanford, R. C. Schroden, M. Al-Daous, and A. Stein, “Gems of chemistry and physics: Macroporous metal oxides with 3D order,” *Adv.Mater.*, vol. 13, pp. 401–407, March 2001.

[3] Y. J. Lee and P. V. Braun, “Tunable inverse opal hydrogel pH sensors”, *Adv. Mater.*, vol. 15, pp. 563-566, April 2003.

[4] S. Fang, H. Wang, J. Yang, S. Lu, B. Yu, J. Wang, and C. Zhao, “Formation of Si nanowires by the electrochemical reduction of porous Ni/SiO2 blocks in molten CaCl2”, *J. Phys. Chem. Solids*, Vol. 89, pp. 1-6, 2016.

[5] P. Jiang, J. F. Bertone, K. S. Hwang, and V. L. Colvin, “Single-crystal colloidal multilayers of controlled thickness”, *Chem. Mater.*, vol. 11, pp. 2132–2140, August 1999.

[6] A. Stein, “Sphere templating methods for periodic porous solids”, *Micropor. Mesopor. Mater.*, vol. 44, pp. 227–239, June 2001.

[7] K. Lee and S.A. Asher, “Photonic crystal chemical sensors: pH andionic strength”, *J. Amer. Chem. Soc.*, vol. 122, pp. 9534–9537, October 2000.

[8] S. Y. Choi, M. Mamak, G. von Freymann, and N. Chopra *et al.*, “Mesoporous Bragg stack color tunable sensors”, *Nano Lett.*, vol. 6, pp. 2456–2461, November 2006.

[9] Z. Wu, D. Lee, M. F. Rubner, and R. E. Cohen, “Structural color in porous, superhydrophilic, and self-cleaning SiO2/TiO2 Bragg stacks”, *Small*, vol. 3, pp. 1445–1451, August 2007.

[10] V. R. Nair and R. Vijaya, "Photonic crystal sensors: An overview", *Prog. Quantum. Electron.*, Vol. 34, No. 3, pp. 89-134, 2010.

[11] N. Doghmosh, S. A. Taya, A. Upadhyay, M. M. Olaimat, and I. Colak, “Enhancement of optical visible wavelength region selective reflector for photovoltaic cell applications using a ternary photonic crystal”, *Optik*, Vol. 243, pp. 167491, 2021.

[12] Y. Ju, “Tolerance analysis of photonic crystal substrate used in spectrometer-free photonic crystal enhanced microscopy”, *Opt. Quantum. Electron.*, vol. 52, pp. 485, 2020.

[13] C. P. Yu, and H. C. Chang, “Applications of the finite difference mode solution method to photonic crystal structures” *Opt. Quantum. Electron.*, 36, pp. 145–163, 2004.

[14] S. Boutami, B. Benbakir, J. Leclercq and P. Viktorovitch, "Compact and polarization controlled 1.55 μm vertical-cavity surface-emitting laser using single-layer photonic crystal mirror", Appl. Phys. Lett., Vol. 91, pp. 071105, 2007.

[15] X. Xu, and J. Ding, “A wide band-pass filter of broad angle incidence based on one-dimensional metallo-dielectric ternary photonic crystal”, *Opt. Quantum. Electron.*, vol. 41, pp. 1027–1032, 2009.

[16] R.G. Bikbaev, S.Y. Vetrov and I.V. Timofeev, "Hyperbolic metamaterial for the Tamm plasmon polariton application", *J. Opt. Soc. Am. B.*, Vol. 37, No. 8, pp. 2215-2220, 2020.

[17] Z. Wang, P. Gao, S. Liu, and X. Chen, “A reflective methane concentration sensor based on biconvex cone photonic crystal fiber”, *Optik*, Vol. 24, pp. 166983, 2021.

[18] J.E. Baker, R. Sriram and B.L. Miller, "Two-dimensional photonic crystals for sensitive microscale chemical and biochemical sensing", *LOC*, Vol. 21, pp. 971–990, 2015.

[19] F. Segovia-Chaves and H. Vinck-Posada, "Dependence of the defect mode with temperature, pressure and angle of incidence in a 1D semiconductor-superconductor photonic crystal", *Phys. C. Supercond. Appl.*, Vol. 553, pp. 1–7, 2018.

[20] F. Frascella, S. Ricciardi, P. Rivolo, V. Moi, F. Giorgis, E. Descrovi, F. Michelotti, P. Munzert, N. Danz, L. Napione, M. Alvaro, F. Bussolino, "A fluorescent onedimensional photonic crystal for label-free biosensing based on Bloch surface waves", Sens., Vol. 13, pp. 2011–2022, 2013.

[21] F. Chaves and H. Posada, "Tuning of the defect mode in a 1D superconductor-semiconductor crystal with hydrostatic pressure dependent frequency of the transverse optical phonons", *Phys. C: Supercond. Appl.*, Vol. 556, pp. 7–13, 2019.

[22] T. Chen, Z. Han, J. Liu and Z. Hong, "Terahertz gas sensing based on a simple one-dimensional photonic crystal cavity with high quality factors", *Appl. Opt.*, Vol. 53, pp. 3454–3458, 2014.

[23] R. Kandyala, S. P. Raghavendra, S. T. Rajasekharan, "Xylene: An overview of its health hazards and preventive measures", *OMPJ*, Vol. 14, No. 1, pp. 1-5, January 2010.

[24] K. Niaz, H. Bahadar, F. Maqbool, and M. Abdollahi, "A review of environmental and occupational exposure to xylene and its health concerns", *EXCLI J.*, Vol. 14, pp. 1167-86, November 2015.

[25] L. Pavesi, C. Mazzoleni, R. Guardini, M. Cazzanelli, V. Pellegrini, and A. Tredicucci, "**Porous-silicon microcavities",** IL NUOVO CIMENTO, *VOL. 18,* No. **10, pp. 1213-1223, 1996.**

[26] I.M. White and X. Fan, "On the performance quantification of resonant refractive index sensors", Opt. Express, Vol. 16, No. 2, pp. 1020-1028, 2008.

[27] M. G. Mardones, P. Cea, M. C. López and C. Lafuente, "Refractive properties of binary mixtures containing pyridinium-based ionic liquids and alkanols", Thermochim. Acta, Vol. 572, pp. 39-44, 2013.

[28] X. Xu, B. Peng, D. Li, J. Zhang, L. M. Wong, Q. Zhang, Sh. Wang and Q. Xiong, "Flexible Visible–Infrared Metamaterials and Their Applications in Highly Sensitive Chemical and Biological Sensing", *ACS Publications*, Vol. 11, No. 8, pp. 3232, 2011.

[29] K Zang, D Zhang, Y Huo, X Chen, C Y Lu, E T Fei1, Th I Kamins1, X Feng, Y Huang and J S Harris, "Microring bio-chemical sensor with integrated low dark current Ge photodetector", *Appl. Phys. Lett*., Vol. 106, pp. 101111, 2015.

[30] Y. S. Lin, "Complementary infrared metamaterials for volatile organic solutions sensing", *Mater. Lett*., Vol. 195, pp. 55, 2017.

[31] H. Muthuganesan, Y. Kar, C. V. Kruijsdijk and Sh. K. Selvaraja, "On-Chip Chemical Sensing Using Slot-Waveguide-Based Ring Resonator', *IEEE Sens. J*., Vol. 20, No. 11, pp. 5970, 2020.

[32] Y. Singh, A. Sadhu and S. K. Raghuwanshi, "Development and Experimental Analysis of Titanium Dioxide (TiO_2) Coated Etched Fiber Bragg Grating Sensor for Chemical Sensing", *IEEE Sens. J*., Vol. 20, No. 15, pp. 8528, 2020.

[33] S. A. Taya, A. Sharma, N. Doghmosh and I. Colak, "Detection of water concentration in ethanol solution using a ternary photonic crystal-based sensor", *Mater. Chem. Phys*., Vol. 279, pp. 125772, 2022.